## Introduction

Pancreatic cancer is a highly aggressive cancer characterized by high invasiveness and acute resistance to chemo- and radiotherapy; consequently, it represents one of the most difficult malignancies to detect and treat.[1–2] Patient prognosis is often dismal due to late diagnosis and a lack of effective therapies. This outlook could be improved by realization of diagnostic tools useful at earlier stages of the disease.

Magnetic resonance imaging (MRI) is a powerful and noninvasive technique for medical imaging of soft tissues. MRI offers clinical feasibility for molecular imaging because it provides superb anatomic resolution and contrast for visualizing tissue morphology and anatomical details of organs in vivo.[3–6] Development of contrast agents has been central to advances in MRI techniques for early diagnosis of cancer and detection of biological processes at the cellular and molecular level. Particularly, superparamagnetic iron oxide nanoparticles are gaining popularity for MRI applications in vivo, due to their low toxicity and excellent magnetic susceptibility. These superparamagnetic iron oxide nanoparticles are extremely effective for promoting proton relaxation with significant capacity to reduce MRI signal, and this effect is further enhanced by using spin echo sequences with a longer echo time ($T_2$-weighted imaging).[7] Thus, the accumulation site of iron oxide nanoparticles exhibits negative enhancement of MRI signals in $T_2$-weighted MR images. In order to enhance the in vivo utility to include use for tumor diagnosis, iron oxide nanoparticles should be highly biocompatible, of appropriate size, and should have sufficiently long blood circulation time to allow for passive tumor accumulation through the enhanced permeability and retention (EPR) effect.[8–10] Surface modification of iron oxide nanoparticles with biocompatible polymers can avoid or effectively reduce recognition by the reticuloendothelial system (RES), thus improving their circulating properties.

Poly(ethylene glycol) (PEG) has found widespread clinical use as a biocompatible, nonspecific protein resistant material that prolongs the circulation time of protein therapeutics.[11–12] PEG-based block copolymers and PEGylated liposomes have been used to improve the stability and pharmacokinetics of iron oxide nanoparticles in the physiological environment.[13–14] Many groups showed negative enhancement at the hypervascular tumor site in tumor-bearing mice using PEG-coated iron oxide nanoparticles and $T_2$-weighted MR imaging.[15–16] We also reported PEG-coated iron oxide nanoparticles with a hydrodynamic diameter of ≈100 nm as a negative contrast agent for successful MR imaging of subcutaneous colon tumor models.[17] However, there are no reports to enhance the MR imaging of pancreatic tumors using PEG-coated iron oxide nanoparticles without targetable biomolecules, because PEG-coated iron oxide nanoparticles developed to date have limited circulation in the blood compartment and are too large to penetrate into pancreatic tumors. In fact, without intraperitoneal administration of transforming growth factor-β (TGF-β) inhibitor, PEG-coated iron oxide nanoparticles (≈100 nm) failed to accumulate into a subcutaneous BxPC3 pancreatic tumor model, which is characterized by hypovascularity and thick fibrosis.[18] We have recently found that the size upper limit of the nanoparticle system for passive targeting to pancreatic tumor models is ≈50 nm (unpublished data). Hence, we hypothesized that with proper control of the size and surface properties of iron oxide based nanoparticles, development of effective $T_2$-weighted MRI contrast agents for in vivo detection of pancreatic tumors could be possible.

Recently, gold-coated superparamagnetic core–shell nanoparticles have attracted considerable attention for biomedical applications.[19–23] Au and iron oxide nanoparticles are known to be biocompatible and have been used extensively for optical- and magnetic-based applications, respectively.[24–25] Furthermore, a gold coating on the magnetic nanoparticles is stable under biological conditions and can be further functionalized with sulfur-containing moieties through Au–S bonding.

In this report, we developed PEG-coated iron-oxide–gold core–shell nanoparticles (PEG-AuIONs) for use as a $T_2$-weighted MRI contrast agent for imaging of pancreatic tumor models. In our method, the overall size of the nanoparticle was controlled by coating iron oxide nanoparticles with Au that allowed for reaction with methoxy-PEG-thiol (MeO-PEG-SH) and subsequent formation of a high-density PEG coating on the surface through Au–S bonding, without the formation of any higher-order assemblies. Our results demonstrated that PEG-AuIONs showed prolonged blood circulation and enhanced MR imaging of subcutaneous colon and orthotopic pancreatic tumor models. These findings suggest that our method, which allows precise control of hydrodynamic size and effective PEG density on the iron-oxide–gold core–shell nanoparticle (AuION), could be a promising method for development of MRI contrast agents for various tumor types including pancreatic cancer.

## Experimental Part

AuION was synthesized with a slight modification of a previously reported method.[20,26] Hydrogen tetrachloroaurate was reduced by oleylamine to form a thin gold layer onto oleylamine and oleic acid stabilized iron oxide nanoparticles. MeO-PEG-SH ($\overline{M}_w$: 2 000) was introduced onto the surface of AuIONs through a sequential coating process in chloroform and then in methanol, followed by a solvent exchange to water. Details of PEG-AuION synthesis and characterization are provided in the Supporting Information (SI). The biodistribution of PEG-AuIONs, including tumor accumulation, was evaluated in tumor-bearing mice by measuring the Au content in blood and tissues using inductively coupled plasma–mass spectrometry (ICP-MS). In vivo MRI was performed using a 4.7 T scanner with mice bearing a subcutaneous colon (C26) or


Macromol. Rapid Commun. 2010, 31, 1521–1528

DOI: 10.1002/marc.201000341

orthotopic pancreatic (MiaPaCa) tumor. All the details regarding physicochemical and biological studies are provided as SI.

## Results and Discussion

### Synthesis of PEG-Coated Iron-Oxide–Gold Core–Shell Nanoparticles (AuION)

Figure 1a shows the schematic representation for preparation of the PEG-AuIONs used in this study. First, nearly monodispersed γ-$Fe_2O_3$ nanoparticles with an average diameter of $10.5 \pm 1.6$ nm were obtained by thermal decomposition of $Fe(CO)_5$ in the presence of the capping agents oleylamine and oleic acid (5:1), under aerobic conditions with a slight modification of a previously reported method.[26] A small amount of oleic acid was added into the reaction mixture to avoid the formation of γ-$Fe_2O_3$ nanoparticles with different shapes. In the next step, Au was coated onto the γ-$Fe_2O_3$ nanoparticle surface by the reduction of $HAuCl_4$ with oleylamine at 140 °C in

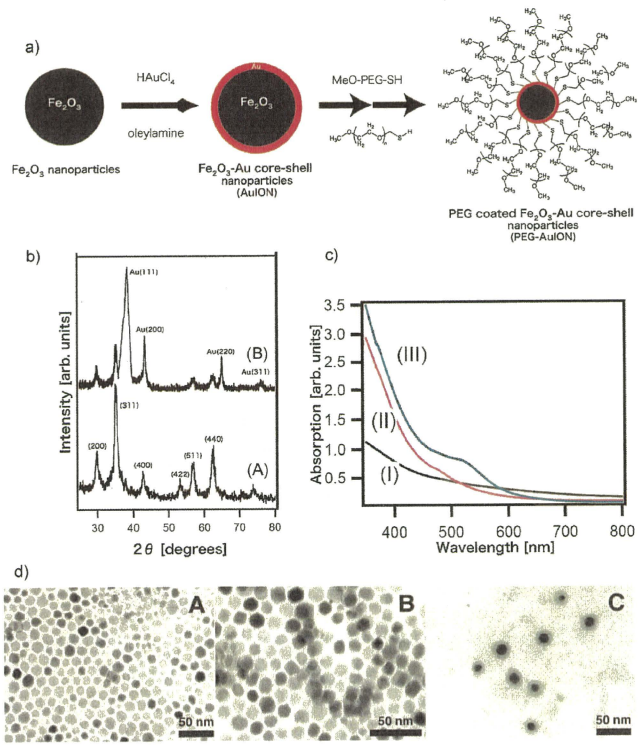


*Figure 1.* Preparation and properties of PEG-AuIONs. a) Scheme for Au shell formation onto γ-$Fe_2O_3$ nanoparticles and subsequent coating with MeO-PEG-SH to form biocompatible PEG-AuIONs. b) X-ray diffraction pattern of γ-$Fe_2O_3$ nanoparticles (A) and AuIONs (B); the Braggs's reflections for both nanoparticles are shown. c) UV–visible spectra of I) γ-$Fe_2O_3$ nanoparticles in chloroform, II) AuIONs in chloroform, and III) PEG-AuIONs in aqueous medium. d) Transmission electron microscopy images of A) γ-$Fe_2O_3$ nanoparticles, B) AuIONs in chloroform, and C) PEG-AuIONs in aqueous medium. The PEG layer is visible on the AuION surface in C. The nanoparticles were stained with 1% phosphotungstic acid solution. The scale bar represents 50 nm in all TEM images.

1,2-dichlorobenzene (ODCB), where oleylamine functions as both the reducing agent and the stabilizer.[21] Oleylamine coated AuIONs were washed by several cycles of dispersion-centrifugation to remove excess oleylamine, and were finally dispersed into chloroform for further modification.

The formation of an Au shell on the $\gamma$-$Fe_2O_3$ nanoparticles was confirmed by X-ray diffraction measurement as shown in Figure 1b. Evolution of Bragg's diffraction peaks from the face-centered cubic (fcc) lattice structure of Au are clearly visible from the X-ray diffraction spectra of AuIONs. Using the Debye–Scherer equation, the thickness of Au on the $\gamma$-$Fe_2O_3$ surface was calculated to be 1.3 nm. Transmission electron microscopy (TEM) studies (Figure 1d(A,B)) showed that the average particle size increased by $1.5 \pm 0.6$ nm following Au deposition onto the $\gamma$-$Fe_2O_3$ nanoparticles, which is comparable to the thickness of Au calculated from the X-ray diffraction peaks.

PEG was readily conjugated to the particle surface by reaction of PEG-SH with the gold surface through well-known thiol–gold coupling chemistry. After a single cycle of PEG modification, followed by the evaporation of chloroform under vacuum, PEG-AuIONs were readily soluble in aqueous medium. However, when the nanoparticles were incubated for 12 h in $150 \times 10^{-3}$ M NaCl solution, agglomeration occurred, suggesting incomplete coating of MeO-PEG-SH on the nanoparticle surface (data not shown). Therefore, repetitive PEG coating onto PEG-AuIONs (described in SI) was performed to increase the PEG density on the particle surface, as it has been reported that the process involving repetitive PEG adsorption significantly contributes to increase the PEG density on the gold surface.[27] Salt-induced agglomeration of PEG-AuIONs obtained by this double PEG coating process was avoided, even after transfer into aqueous media through dialysis, suggesting the formation of a PEG layer with appreciably high density around the AuION surface. PEG-AuIONs stored in $10 \times 10^{-3}$ M Tris-HCl buffer containing 0.03% bovine serum albumin were stable for several months without any notable aggregation. Use of methanol as the solvent for the second cycle of PEG coating also proved to be crucial for controlling particle size and dispersity of the PEGylated nanoparticles, as application of the second PEG coating onto the AuIONs in water resulted in low quality particles with large hydrodynamic diameter and high polydispersity index (data not shown).

The formation of an Au shell on the $\gamma$-$Fe_2O_3$ surface was further confirmed by UV–vis spectroscopy of the PEG-AuION in aqueous medium. As shown in Figure 1c, AuIONs did not show any characteristic plasmon resonance in organic medium as AuIONs are protected by the long chain alkyl ligands. However, when the AuION was transferred to the aqueous medium as a PEGylated nanoparticle, a plasmon resonance band appears with absorption at 515 nm, probably due to the increased dielectric constant of the medium.

## Characterization of PEG-Coated Iron-Oxide–Gold Core–Shell Nanoparticles (PEG-AuION)

The TEM image of PEG-AuION transferred to water after surface modification with MeO-PEG-SH (Figure 1d(C)) showed no apparent agglomeration. Furthermore, the PEG layer surrounding the AuION core was visible in TEM after negative staining with 1% phosphotungstic acid as seen in Figure 1d(C). The thickness of the PEG layer was determined to be $6.5 \pm 1.2$ nm from this TEM image.

The neutral $\zeta$-potential of $0.49 \pm 0.12$ mV of PEG-AuIONs in water showed complete passivation of the nanoparticle surface with the PEG layer. The number of PEG molecules (molecular weight = 2 kDa) on the surface of a single 12.9 nm AuION was calculated to be ~2500 by thermogravimetric analysis (TGA) analysis of the sample under $N_2$ atmosphere. This surface coverage corresponds to a footprint area of 0.25 $nm^2$ per PEG molecule, which is significantly smaller than previous reports for MeO-PEG-SH conjugated on Au nanoparticle surfaces (2.42 $nm^2$).[28–29] This result suggests that the PEG-AuION possesses an appreciably dense PEG layer. Chain conformation of grafted PEG on a surface plane is estimated to be an extended brush at this density (0.25 $nm^2$). Nevertheless, on a spherical surface, PEG density decreases in a radial direction toward the exterior of the particle with a change in the PEG conformation from brush to random coil (a mushroom model).[30] Note that the height of PEG 2kDa in a mushroom conformation is estimated to be 3.3 nm (twice of radius of gyration ($R_g$)) as lower limit,[31] whereas the height in an extended conformation is estimated to be 15.9 nm as upper limit by using the effective monomer length of PEG in water ($2000/44 \times 0.35 = 15.9$ nm).[32] The PEG thickness estimated from the TEM image for PEG-AuIONs obtained in this study ($6.5 \pm 1.2$ nm) is in the range between these lower and upper estimated heights of PEG in the extended brush and random coil conformation.

The dispersion stability of PEG-AuIONs against increased NaCl concentration in aqueous solution was evaluated by dynamic light scattering (DLS) measurement, which revealed that the hydrodynamic diameter remained constant up to 1 M NaCl (Figure 2a). Furthermore, there was no change in the diameter of PEG-AuIONs even after 12 h incubation in $10 \times 10^{-3}$ M Tris-HCl buffer containing 10% fetal bovine serum at pH 7.4 and 37 °C (Figure 2b). PEG-AuIONs were also found to be stable in buffer within the pH range of 3–10.

To examine the feasibility of PEG-AuIONs as a $T_2$-weighted MRI contrast agent, we evaluated the relaxivity $r_2$ of PEG-AuIONs and determined the value to be $149.32 \times 10^{-3}\ M^{-1} \cdot s^{-1}$ (Figure 2c). This $r_2$ value is comparable to the commercially


Macromol. Rapid Commun. 2010, 31, 1521–1528

DOI: 10.1002/marc.201000341

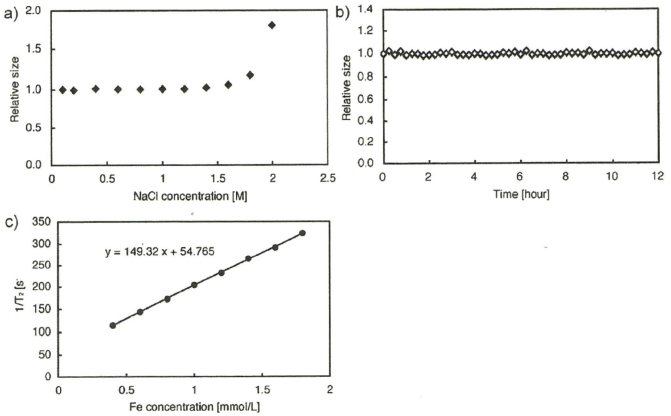


*Figure 2.* a) Change in the relative particle size of PEG-AuIONs with increased NaCl concentration, determined by DLS measurement. b) Time-dependency of the relative size of PEG-AuIONs in Tris-HCl buffer containing 10% fetal bovine serum at 37 °C. c) Relaxivity $r_2$ of PEG-AuIONs using the Carr-Purcell-Meiboom-Gill (CPMG) pulse sequence at 25 °C, 0.59 T.

available $T_2$ contrast agent Feridex (dextran-coated iron oxide nanoparticles).

### Biodistribution of PEGylated Fe2O3-Au Core–Shell Nanoparticles

Figure 3 shows the concentration of gold in blood plasma over time after intravenous administration of PEG-AuIONs. The gold concentration measured in plasma indicates that PEG-AuIONs stably circulate in the blood compartment with 8% of the injected dose observed even after 24 h. Prolonged blood circulation of the PEG-AuION was reasonably associated with high stability of PEG-AuIONs under physiological conditions at 37 °C (Figure 2). Accumulation of PEG-AuIONs within solid tumor and normal tissues (liver, kidney, spleen and muscle) is also shown in Figure 3. Notably, PEG-AuION showed continuous accumulation with time into solid tumors, while its accumulation to other tissues was somewhat limited.

To assess the selectivity towards the solid tumors, the area under the Au concentration–time curve (AUC) and AUC ratios of the tumor to normal tissues at 24 h after injection were determined and are shown in Supplementary Table 1 in the SI. PEG-AuIONs exhibited ratios $AUC_{tumor}/AUC_{organ} > 1.0$ for spleen, kidney, and muscle tissues, indicating selectivity to the tumor ($AUC_{tumor}/AUC_{organ}$ of 2.84, 1.21, and 67.27 for spleen, kidney, and muscle tissues, respectively). These $AUC_{tumor}/AUC_{organ}$ ratios are comparable to those observed for so-called stealth drug carriers.[33] However, $AUC_{tumor}/AUC_{liver}$ ratio is somewhat low at 0.95. This may be due to the relatively high blood volume in the liver. Note that liver has about one-fifth of blood volume in the body, and the liver accumulation value for PEG-AuIONs has a substantial contribution from PEG-AuIONs present in the blood pool.

### In vivo Tumor Imaging

In order to study the efficacy of PEG-AuIONs for dynamic in vivo MRI, imaging of tumor tissue was conducted and compared with the commercially available MRI contrast agent Feridex (dextran-coated iron oxide nanoparticles). First, we performed in vivo MRI with nude mice bearing subcutaneously inoculated murine colon adenocarcinoma (C26) cells (Figure 4a,b). Negative enhancement of the tumor site in $T_2$-weighted images, which is indicated as circled by red line in Figure 4, gradually increased 5 min after injection of PEG-AuIONs, with a maximum negative enhancement of 60% observed at 4 h post-injection (Figure 4a,e and Table 1). Note that MRI signals in other organs and tissues surrounding the tumor were also negatively enhanced in $T_2$-weighted images due to the existence of high concentration of PEG-AuIONs in the blood circulation. Therefore, the percentile rates of negative enhancement at 4 h post-injection of PEG-AuIONs were compared between in the tumor and the intestine

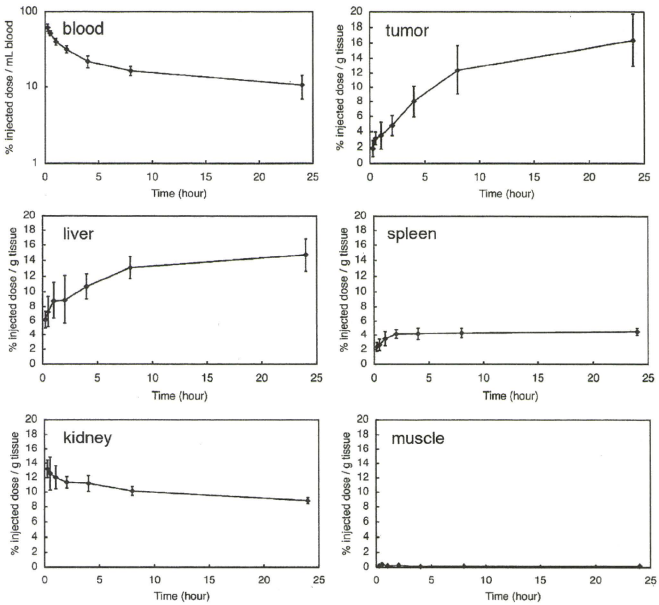


*Figure 3.* Biodistribution of PEG-AuIONs. The levels of Au in blood, tumor, liver, spleen, kidney, and muscles are shown as percentage of dose at each time after intravenous injection.

(indicated as circled by yellow line in MR images) (Table 1), suggesting that PEG-AuIONs reduced MRI signals more efficiently in the tumor compared with intestine. In contrast, Feridex failed to reduce MRI signals selectively in the tumor even after 4 h (Figure 4b,e and Table 1), presumably due to non-specific accumulation in the RES.

Next, we tested the efficacy of the PEG-AuIONs in an orthotopic pancreatic cancer model, using MiaPaCa-2 cells derived from human pancreatic cancer. The $T_2$-weighted MR images of the tumor region over time are shown in Figure 4c,d. Noticeable negative enhancement (~25%) was observed as soon as 5 min after administration of PEG-AuIONs, and continued even 4 h after administration (Figure 4c,f and Table 2). It should be noted that PEG-AuIONs exhibited focal MRI signal enhancement in the tumor tissue (indicated by red arrowhead in Figure 4c), presumably due to their heterogeneous intratumoral distribution. The rate of negative enhancement in those regions was calculated to be 47%, which was appreciably higher than that in the intestine (18%) (Table 2). In contrast, Feridex failed in the tumor-selective MRI signal enhancement in this model (Figure 4d,f and Table 2). Furthermore, we tested the effects of the PEG-AuION system compared to Feridex in a model representing metastatic foci in the liver using MiaPaCa-2 cells (Supplementary Figure 1a,b and Supplementary Table 2 in the SI), and the results were consistent with those obtained in the orthotopic model described above. The accumulation of PEG-AuIONs in

*Table 1.* Percentile rate of negative enhancement in MR signals in the tumor and intestine at 4 h post-injection of PEG-AuION and Feridex into mice bearing a subcutaneous model of murine colon adenocarcinoma (C26) celles.

| | Negative enhancement in MRI signals | |
|---|---|---|
| | Tumor | Intestine |
| PEG-AuION | 60% | 25% |
| Feridex | 5% | 8% |


*Macromol. Rapid Commun.* **2010**, *31*, 1521–1528

Macromolecular Journals

DOI: 10.1002/marc.201000341

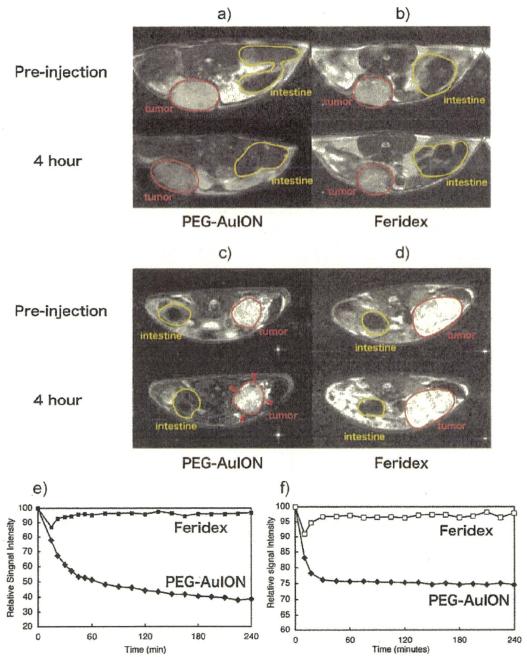


*Figure 4.* In vivo MR imaging of tumors. a,b) $T_2$-weighted images of subcutaneous C26 murine carcinoma (tumor sites are circled by red line) at 4 h after intravenous injection of PEG-AuIONs (a) and Feridex (b). c,d) $T_2$-weighted images of an orthotopic MiaPaCa-2 human pancreatic cancer model (tumor sites are circled by red line) at 4 h after intravenous injection of PEG-AuIONs (c) and Feridex (d). All images were obtained in a magnetic field strength of 4.7 T. Time-dependencies of relative signal intensities at the tumor site in $T_2$-weighted images after injection of PEG-AuIONs and Feridex in C26 subcutaneous tumor model (e) and in MiaPaCa-2 orthotopic tumor model (f).

metastatic foci was confirmed histologically using silver staining against gold particles (Supplementary Figure 1c in the SI). These results suggest successful MR imaging of malignant tumors is feasible using PEG-AuIONs.

## Conclusion

In this study, we have demonstrated that AuIONs of sub-50-nm size and coated with a dense PEG brush can be used as an MRI contrast agent for a variety of tumors, including pancreatic tumors. The relatively small hydrodynamic diameter along with a high PEG density facilitated extended circulation of PEG-AuIONs, which allowed for accumulation into pancreatic cancer models through the EPR effect. These results imply that with proper control of the structural and surface properties of the nanoparticles, it is feasible to develop effective MRI contrast agents for the diagnosis of intractable tumors such as pancreatic cancer, even without attachment of cell-targeting ligands. The presence of an Au shell on the magnetic nanoparticle not only offers the possibility for surface modification with various biomolecules for biomarker-targeted imaging, but also offers another detection modality through various techniques such as X-ray tomography[34–35] (CT) and surface-enhanced Raman scattering (SERS).[36] The ultimate goal of nanoparticle materials for medical research is to develop high-performance systems for both detection and treatment of biological events such as cancer metastasis and real-time visualization of biological events at the cellular and molecular level,

*Table 2.* Percentile rate of negative enhancement in MR signals in the tumor and intestine at 4 h post-injection of PEG-AuION and Feridex into mice bearing an orthotopic model of human pancreatic adenocarcinoma (MiaPaCa-2) cells.

| | Negative enhancement in MRI signals | | |
|---|---|---|---|
| | Tumor (whole) | Tumor (arrow head[a)]) | Intestine |
| PEG-AuION | 25% | 47% | 18% |
| Feridex | 3% | – | 6% |

[a)]The rate of negative enhancement of MRI signals in the regions indicated by red arrowhead in Figure 4c was calculated.

leading to better prognosis in patients bearing tumor. The results of this study represent a significant improvement in nanoparticle-based tumor detection, which may prove useful for clinical applications and also in the design of more advanced systems.

Acknowledgements: The authors thank Dr. *James R. Christie II*, The University of Tokyo, for editing the English of the manuscript. This research was supported by the *Japan Society for the Promotion of Science (JSPS)* through its "Funding Program for World-Leading Innovative R&D on Science and Technology (FIRST Program)". We are grateful to Dr. *S. Fukuda*, The University of Tokyo Hospital, for his valuable support in the TEM measurement. T. K. S. acknowledges a fellowship from the *Japan Society for the Promotion of Science (JSPS)*.

Received: June 8, 2010; Revised: June 30, 2010; DOI: 10.1002/marc.201000341

Keywords: gold coatings; iron oxide; magnetic resonance imaging; nanoparticles; poly(ethylene glycol)

[1] A. Jemal, R. Siegel, E. Ward, Y. P. Hao, J. Q. Xu, M. J. Thun, *CA-A Cancer Journal For Clinicians* **2009**, *59*, 225.
[2] M. J. MacKenzie, *Lancet Oncology* **2004**, *5*, 541.
[3] R. Weissleder, A. Moore, U. Mahmood, R. Bhorade, H. Benveniste, E. A. Chiocca, J. P. Basilion, *Nat. Med.* **2000**, *6*, 351.
[4] H. B. Na, I. C. Song, T. Hyeon, *Adv. Mater.* **2009**, *21*, 1.
[5] Y. W. Jun, J. H. Lee, J. Cheon, *Angew. Chem., Int. Ed.* **2008**, *47*, 5122.
[6] S. Laurent, D. Forge, M. Port, A. Roch, C. Robic, L. V. Elst, R. N. Muller, *Chem. Rev.* **2008**, *108*, 2064.
[7] Y. J. Wang, S. M. Hussain, G. P. Krestin, *Eur. Radiol.* **2001**, *11*, 2319.
[8] Y. Matsumura, H. Maeda, *Cancer Res.* **1986**, *46*, 6387.
[9] H. Maeda, J. Fang, T. Inutsuka, Y. Kitamoto, *Int. Immunopharmacol.* **2003**, *3*, 319.
[10] D. M. McDonald, P. Baluk, *Cancer Res.* **2002**, *62*, 5381.
[11] J. M. Harris, R. B. Chess, *Nat. Rev Drug Discov.* **2003**, *2*, 214.
[12] K. Kataoka, A. Harada, Y. Nagasaki, *Adv. Drug. Delivery Rev.* **2001**, *47*, 113.
[13] C. Khemtong, C. W. Kessinger, J. M. Ren, E. A. Bey, S. G. Yang, J. S. Guthi, D. A. Boothman, A. D. Sherry, J. M. Gao, *Cancer Res.* **2009**, *69*, 1651.
[14] J. F. Berret, N. F. Schonbeck, F. Gazeau, D. El Kharrat, O. Sandre, A. Vacher, M. Airiau, *J. Am. Chem. Soc.* **2006**, *128*, 1755.
[15] H. Lee, M. K. Yu, S. Park, S. Moon, J. J. Min, Y. Y. Jeong, H.-W. Kang, S. Jon, *J. Am. Chem. Soc.* **2007**, *129*, 12739.
[16] E. K. U. Larsen, T. Nielsen, T. Wittenborn, H. Birkedal, T. Vorup-Jensen, M. H. Jakobsen, L. Østergaard, M. R. Horsman, F. Besenbacher, K. A. Howard, J. Kjems, *ACS Nano*, **2009**, *3*, 1947.
[17] M. Kumagai, Y. Imai, M. T. Nakamura, Y. Yamasaki, M. Sekino, S. Ueno, K. Hanaoka, K. Kikuchi, T. Nagano, E. Kaneko, K. Shimokado, K. Kataoka, *Colloids Surf. B* **2007**, *56*, 174.
[18] M. Kumagai, M. R. Kano, Y. Morishita, M. Ota, Y. Imai, N. Nishiyama, M. Sekino, S. Ueno, K. Miyazono, K. Kazunori, *J. Control. Release* **2009**, *140*, 306.
[19] J. L. Lyon, D. A. Fleming, M. B. Stone, P. Schiffer, M. E. Williams, *Nano Lett.* **2004**, *4*, 719.
[20] L. Y. Wang, J. Luo, Q. Fan, M. Suzuki, I. S. Suzuki, M. H. Engelhard, Y. H. Lin, N. Kim, J. Q. Wang, C. J. Zhong, *J. Phys. Chem. B* **2005**, *109*, 21593.
[21] Z. Xu, Y. Hou, S. Sun, *J. Am. Chem. Soc.* **2007**, *129*, 8698.
[22] D. Kim, J. W. Kim, Y. Y. Jeong, S. Jon, *Bull. Korean Chem. Soc.* **2009**, *30*, 1855.
[23] H. Kojima, Y. Mukai, M. Yoshikawa, K. Kamei, T. Yoshikawa, M. Morita, T. Inubushi, T. A. Yamamoto, Y. Yoshioka, N. Okada, S. Seino, S. Nakagawa, *Bioconjugate Chem.* **2010**, *21*, 1026.
[24] S.-I. Cho, B. R. Jarrett, A. Y. Louie, S. M. Kauzlarich, *Nanotechnology* **2006**, *17*, 640.
[25] T. A. Larson, J. Bankson, J. Aaron, K. Sokolov, *Nanotechnology* **2007**, *18*, 325101.
[26] J. W. Cheon, N. J. Kang, S. M. Lee, J. H. Lee, J. H. Yoon, S. J. Oh, *J. Am. Chem. Soc.* **2004**, *126*, 1950.
[27] K. Uchida, H. Otsuka, M. Kaneko, K. Kataoka, Y. Nagasaki, *Anal. Chem.* **2005**, *77*, 1075.
[28] S. Takae, Y. Akiyama, H. Otsuka, T. Nakamura, Y. Nagasaki, K. Kataoka, *Biomacromolecules* **2005**, *6*, 818.
[29] W. P. Wuelfing, S. M. Gross, D. T. Miles, R. W. Murray, *J. Am. Chem. Soc.* **1998**, *120*, 12696.
[30] K. Ohno, T. Morinaga, S. Takeno, Y. Tsujii, T. Fukuda, *Macromolecules* **2007**, *40*, 9143.
[31] S. Kawaguchi, G. Imai, J. Suzuki, A. Miyahara, T. Kitano, K. Ito, *Polymer* **1997**, *38*, 2885.
[32] A. K. Kenworthy, K. Hristova, D. Needham, T. J. McIntosh, *Biophys. J.* **1995**, *68*, 1921.
[33] H. Cabral, N. Nishiyama, K. Kataoka, *J. Controlled Release* **2007**, *121*, 146.
[34] Q. Y. Cai, S. H. Kim, K. S. Choi, S. Y. Kim, S. J. Byun, K. W. Kim, S. H. Park, S. K. Juhng, K. H. Yoon, *Investigative Radiology* **2007**, *42*, 797.
[35] D. Kim, S. Park, J. H. Lee, Y. Y. Jeong, S. Jon, *J. Am. Chem. Soc.* **2007**, *129*, 7661.
[36] X. Qian, X. H. Peng, D. O. Ansari, Q. Yin-Goen, G. Z. Chen, D. M. Shin, L. Yang, A. N. Young, M. D. Wang, S. M. Nie, *Nat. Biotechnol.* **2008**, *26*, 83.


*Macromol. Rapid Commun.* **2010**, *31*, 1521–1528

DOI: 10.1002/marc.201000341

molecular pharmaceutics

articles

# Antiangiogenic Gene Therapy of Solid Tumor by Systemic Injection of Polyplex Micelles Loading Plasmid DNA Encoding Soluble Flt-1

**Makoto Oba,[†] Yelena Vachutinsky,[‡] Kanjiro Miyata,[§] Mitsunobu R. Kano,[∥,⊥] Sorato Ikeda,[#] Nobuhiro Nishiyama,*[,§] Keiji Itaka,[§] Kohei Miyazono,[∥,⊥] Hiroyuki Koyama,[†] and Kazunori Kataoka*[,‡,§,∥,#]**

*Department of Clinical Vascular Regeneration, Graduate School of Medicine, The University of Tokyo, 7-3-1 Hongo, Bunkyo, Tokyo 113-8655, Japan, Department of Bioengineering, Graduate School of Engineering, The University of Tokyo, 7-3-1 Hongo, Bunkyo, Tokyo 113-8656, Japan, Center for Disease Biology and Integrative Medicine, Graduate School of Medicine, The University of Tokyo, 7-3-1 Hongo, Bunkyo, Tokyo 113-0033, Japan, Center for NanoBio Integration, The University of Tokyo, 7-3-1 Hongo, Bunkyo, Tokyo 113-8656, Japan, Department of Molecular Pathology, Graduate School of Medicine, The University of Tokyo, 7-3-1 Hongo, Bunkyo-ku, Tokyo 113-8655, Japan, and Department of Materials Engineering, Graduate School of Engineering, The University of Tokyo, 7-3-1 Hongo, Bunkyo, Tokyo 113-8656, Japan*

Received September 14, 2009; Revised Manuscript Received January 8, 2010; Accepted February 23, 2010

**Abstract:** In this study, a polyplex micelle was developed as a potential formulation for antiangiogenic gene therapy of subcutaneous pancreatic tumor model. Poly(ethylene glycol)-poly(L-lysine) block copolymers (PEG-PLys) with thiol groups in the side chain of the PLys segment were synthesized and applied for preparation of disulfide cross-linked polyplex micelles through ion complexation with plasmid DNA (pDNA) encoding the soluble form of vascular endothelial growth factor (VEGF) receptor-1 (sFlt-1), which is a potent antiangiogenic molecule. Antitumor activity and gene expression of polyplex micelles with various cross-linking rates were evaluated in mice bearing subcutaneously xenografted BxPC3 cell line, derived from human pancreatic adenocarcinoma, and polyplex micelles with optimal cross-linking rate achieved effective suppression of tumor growth. Significant gene expression of this micelle was detected selectively in tumor tissue, and its antiangiogenic effect was confirmed by decreased vascular density inside the tumor. Therefore, the disulfide cross-linked polyplex micelle loading sFlt-1 pDNA has a great potential for antiangiogenic therapy against subcutaneous pancreatic tumor model by systemic application.

**Keywords:** Polymeric micelle; block copolymer; antiangiogenic tumor gene therapy; sFlt-1

## Introduction

Antiangiogenic tumor gene therapy is an intensively studied approach to inhibit tumor growth by destructing its neo-vasculature formation.[1,2] Vascular endothelial growth factor (VEGF) is a major proangiogenic molecule, which stimulates angiogenesis via promoting endothelial prolifera-

* To whom correspondence should be addressed. K.K.: tel, +81-3-5841-7138; fax, +81-3-5841-7139; e-mail, kataoka@bmw.t.u-tokyo.ac.jp; The University of Tokyo, Department of Materials Engineering, 7-3-1 Hongo, Bunkyo-ku, Tokyo 113-8656, Japan. N.N.: tel, +81-3-5841-1430; fax, +81-5841-7139; e-mail, nishiyama@bmw.t.u-tokyo.ac.jp.

[†] Department of Clinical Vascular Regeneration, Graduate School of Medicine.

[‡] Department of Bioengineering, Graduate School of Engineering.

[§] Center for Disease Biology and Integrative Medicine, Graduate School of Medicine.

[∥] Center for NanoBio Integration.

[⊥] Department of Molecular Pathology, Graduate School of Medicine.

[#] Department of Materials Engineering, Graduate School of Engineering.

10.1021/mp9002317 © 2010 American Chemical Society
Published on Web 02/23/2010

tion, survival, and migration. The soluble form of VEGF receptor-1 (fms-like tyrosine kinase-1: Flt-1) is a potent endogeneous molecule, which can be used for antiangiogenic therapy.[3,4] The sFlt-1 binds to VEGF with the same affinity and equivalent specificity as that of the original receptor,[5] however it inhibits its signal transduction.

Gene therapy is becoming a promising strategy to supply consecutive expression of antiangiogenic proteins over a period of time. Indeed, a number of studies have already demonstrated the potential of therapeutic genes encoding angiogenic inhibitors to suppress tumor growth.[6,7] The major challenge in systemic gene therapy, however, is a need for a safe and effective vector system that can deliver the gene to the target tissue and cells with no detrimental side effects. In terms of safety, nonviral gene vectors are gaining popularity over viral vectors, however, their intracellular delivery and transfection potential require further optimization. Recently, several reports were published on *in vivo* nonviral gene therapy utilizing sFlt-1 for inhibition of tumor angiogenesis.[8,9]

Based on these criteria, cross-linked polyplex micelles were designed and prepared through electrostatic interaction of thiolated poly(ethylene glycol)-poly(L-lysine) (PEG-PLys) block copolymers and plasmid DNA (pDNA) encoding sFlt-1. We have previously reported that disulfide cross-links introduced into the polyplex micelle core contribute to the stabilization of its structure in the extracellular entity while facilitating smooth release of the entrapped pDNA, in response to the reductive environment, inside the cells.[10,11] The outer hydrophilic shell layer, formed by PEG segment, increases complex stability in serum, avoiding nonspecific interactions with plasma proteins and reduces polymer toxicity.[12]

In this study, cross-linked polyplex micelles were systemically administered to mice bearing subcutaneously xenografted BxPC3 human pancreatic adenocarcinoma and evaluated for their transfection efficiency. Note that BxPC3 xenografts, as some intractable solid tumors, are characterized by stroma-rich histology,[13] which limits access of therapeutic agents to tumor cells. Thus, the accessibility of endothelial cells by bloodstream makes an antiangiogenic approach an attractive strategy against this model. Here we report a potent tumor growth inhibitory effect achieved by effective antiangiogenic ability by the polyplex micelles with an optimal cross-linking degree, which enables the selective expression of loaded sFlt-1 gene in tumor tissue.

## Experimental Section

**Materials.** pDNA for luciferase (Luc) with the pCAcc vector having the CAG promoter was provided by RIKEN Gene Bank (Tsukuba, Japan) and amplified in competent DH5α *Escherichia coli*, followed by purification using a NucleoBond Xtra Maxi (Machery-Nagel GmbH & Co. KG, Düren, Germany). Dulbecco's modified Eagle's medium (DMEM) and RPMI 1640 medium were purchased from Sigma-Aldrich Co. (Madison, WI). Fetal bovine serum (FBS) was purchased from Dainippon Sumitomo Pharma Co., Ltd. (Osaka, Japan). Alexa488- and Alexa647-conjugated secondary antibodies to rat IgG were obtained from Invitrogen Molecular Probes (Eugene, OR). Human soluble VEGF R1/


(1) Folkman, J. Tumor Angiogenesis: Therapeutic Implications. *N. Engl. J. Med.* **1971**, *285*, 1182–1186.

(2) Quesada, A. R.; Munoz-Chapuli, R.; Medina, M. A. Anti-angiogenic Drugs: from Bench to Clinical Trials. *Med. Res. Rev.* **2006**, *26*, 483–530.

(3) Shibuya, M.; Yamaguchi, S.; Yamane, A.; Ikeda, T.; Tojo, A.; Matsushime, H.; Sato, M. Nucleotide Sequence and Expression of a Novel Human Receptor-type Tyrosine Kinase Gene (flt) Closely Related to the Fms Family. *Oncogene* **1990**, *5*, 519–524.

(4) Kendall, R. L.; Thomas, K. A. Inhibition of Vascular Endothelial Cell Growth Factor Activity by an Endogenously Encoded Soluble Receptor. *Proc. Natl. Acad. Sci. U.S.A.* **1993**, *90*, 10705–10709.

(5) Kendall, R. L.; Wang, G.; Thomas, K. A. Identification of a Natural Soluble Forma of the Vascular Endothelial Growth Factor Receptor, FLT-1, and Its Heterodimerization with KDR. *Biochem. Biophys. Res. Commun.* **1996**, *226*, 324–428.

(6) Kong, H. L.; Hecht, D.; Song, W.; Kovesdi, I.; Hackett, N. R.; Yayon, A.; Crystal, R. G. Regional Suppression of Tumor Growth by In Vivo Transfer of a cDNA Encoding a Secreted form of the Extracellular Domain of the Flt-1 Vascular Endothelial Growth Factor Receptor. *Hum. Gene Ther.* **1998**, *9*, 823–833.

(7) Kuo, C. J.; Farnebo, F.; Yu, E. Y.; Christofferson, R.; Swearingen, R. A.; Charter, R.; von Recum, H. A.; Yuan, J.; Kamihara, J.; Flynn, E.; D' Amato, R.; Folkman, J.; Mulligan, R. C. Comparative Evaluation of the Antitumor Activity of Antiangiogenic Proteins Delivered by Gene Transfer. *Proc. Natl. Acad. Sci. U.S.A.* **2001**, *98*, 4605–4610.

(8) Kim, W. J.; Yockman, J. W.; Jeong, J. H.; Christensen, L. V.; Lee, M.; Kim, Y. H.; Kim, S. W. Anti-angiogenic Inhibition of Tumor Growth by Systemic Delivery of PEI-g-PEG-RGD/pCMV-sFlt-1 Complexes in Tumor-bearing Mice. *J. Controlled Release* **2006**, *114*, 381–388.

(9) Kommareddy, S.; Amiji, M. Antiangiogenic Gene Therapy with Systemically Administered sFlt-1 Plasmid DNA in Engineered Gelatin-based Nanovactors. *Cancer Gene Ther.* **2007**, *14*, 488–498.

(10) Miyata, K.; Kakizawa, Y.; Nishiyama, N.; Harada, A.; Yamasaki, Y.; Koyama, H.; Kataoka, K. Block Catiomer Polyplexes with Regulated Densities of Charge and Disulfide Cross-linking Directed to Enhance Gene Expression. *J. Am. Chem. Soc.* **2004**, *126*, 2355–2361.

(11) Miyata, K.; Kakizawa, Y.; Nishiyama, N.; Yamasaki, Y.; Watanabe, T.; Kohara, M.; Kataoka, K. Freeze-dried Formulations for *In Vivo* Gene Delivery of PEGylated Polyplex Micelles with Disulfide Crosslinked Cores to the Liver. *J. Controlled Release* **2005**, *109*, 15–23.

(12) Itaka, K.; Yamauchi, K.; Harada, A.; Nakamura, K.; Kawaguchi, H.; Kataoka, K. Polyion Complex Micelles from Plasmid DNA and Poly(ethylene glycol)-poly(L-lysine) Block Copolymer as Serum-tolerable Polyplex System: Physicochemical Properties of Micelles Relevant to Gene Transfection Efficiency. *Biomaterials* **2003**, *24*, 4495–4506.

(13) Kano, M. R.; Bae, Y.; Iwata, K.; Morishita, Y.; Yashiro, M.; Oka, M.; Fujii, T.; Komuro, A.; Kiyono, K.; Kaminishi, M.; Hirakawa, K.; Ouchi, Y.; Nishiyama, N.; Kataoka, K.; Miyazono, K. Improvement of Cancer-targeting Therapy, Using Nanocarriers for Intractable Solid Tumors by Inhibition of TGF-beta Signaling. *Proc. Natl. Acad. Sci. U.S.A.* **2007**, *104*, 3460–3465.

Flt-1 immunoassay kit was purchased from R&D Systems, Inc. (Minneapolis, MN). Gemcitabine was obtained from Eli Lilly and Company (Indianapolis, IN). Avastin was obtained from F. Hoffmann-La Roche, Ltd. (Basel, Switzerland). Synthesis of thiolated block copolymer, and construction and confirmation of pDNA encoding sFlt-1 are shown in the Supporting Information. A block copolymer with *X*% of thiolation degree was abbreviated as "B-SH*X*%".

**Cell Lines and Animals.** Human embryonic kidney 293T cells (from RIKEN CELL BANK, Tsukuba, Japan) and human pancreatic adenocarcinoma BxPC3 cells (from ATCC, Manassas, VA) were maintained in DMEM and RPMI medium, respectively, supplemented with 10% FBS in a humidified atmosphere containing 5% $CO_2$ at 37 °C. 293T cells were chosen for *in vitro* experiments as cells that did not express sFlt-1.[14] Balb/c nude mice (female, 5 weeks old) were purchased from Charles River Laboratories (Tokyo, Japan). All animal experimental protocols were performed in accordance with the Guide for the Care and Use of Laboratory Animals as stated by the National Institutes of Health.

**Preparation of Polyplex Micelles.** Each block copolymer was dissolved in 10 mM Tris-HCl buffer (pH 7.4), followed by the addition of 10-times-excess mol of dithiothreitol (DTT) against thiol groups. After 30 min incubation at room temperature, the polymer solution was added to a twice-excess volume of 225 μg/mL pDNA/10 mM Tris-HCl (pH 7.4) solution to form polyplex micelles with N/P ratio = 2. Note that N/P ratio was defined as the residual molar ratio of amino groups of thiolated PEG-PLys to phosphate groups of pDNA. The final pDNA concentration was adjusted to 150 μg/mL. After overnight incubation at room temperature, the polyplex micelle solution was dialyzed against 10 mM Tris-HCl buffer (pH 7.4) containing 0.5 vol% DMSO at 37 °C for 24 h to remove the impurities, followed by 24 h of additional dialysis against 10 mM Tris-HCl buffer (pH 7.4) or 10 mM Hepes buffer (pH 7.4) to remove DMSO. During the dialysis, the thiol groups of thiolated block copolymers were oxidized to form disulfide cross-links. In the *in vivo* experiments, the polyplex micelle solution was adjusted to a concentration of 100 μg of pDNA/mL in 10 mM Hepes buffer (pH 7.4) with 150 mM NaCl.

**Dynamic Light Scattering (DLS) Measurement.** The size of the polyplex micelles was evaluated by DLS using Nano ZS (ZEN3600, Malvern Instruments, Ltd., U.K.). A He−Ne ion laser (633 nm) was used as the incident beam. Polyplex micelle solutions with N/P = 2 from 3 different batches were adjusted to a concentration of 33.3 μg of pDNA/mL in 10 mM Tris-HCl buffer (pH 7.4). The data obtained at a detection angle of 173° and a temperature of 37 °C were analyzed by a cumulant method to obtain the hydrodynamic diameters and polydispersity indices ($\mu/\Gamma^2$) of micelles.

**Zeta-Potential Measurement.** The zeta-potential of polyplex micelles was evaluated by the laser-Doppler electrophoresis method using Nano ZS with a He−Ne ion laser (633 nm). Polyplex micelle solutions with N/P = 2 from 3 different batches were adjusted to a concentration of 33.3 μg pDNA/mL in 10 mM Tris-HCl buffer (pH 7.4). The zeta-potential measurements were carried out at 37 °C. A scattering angle of 173 °C was used in these measurements.

**Real-Time Gene Expression.** 293T cells (100,000 cells) were seeded on a 35 mm dish and incubated overnight. After replacement with fresh medium containing 0.1 mM D-luciferin, each type of polyplex micelle (N/P = 2) containing 3 μg of Luc pDNA was added. The dishes were set in a luminometer incorporated in a $CO_2$ incubator (AB-2550 Kronos Dio, ATTO, Tokyo, Japan), and the bioluminescence was monitored every 10 min with an exposure time of 1 min. Reproducibility was confirmed by triplicate experiments.

**Antitumor Activity Assay.** Balb/c nude mice were inoculated subcutaneously with BxPC3 cells ($5 \times 10^6$ cells in 100 μL of PBS). Tumors were allowed to grow for 2−3 weeks to reach the proliferative phase (the size of the tumors at this point was approximately 60 $mm^3$). Subsequently, polyplex micelles (20 μg of pDNA/mouse), gemcitabine (100 mg/kg), or Avastin (50 mg/kg) maintained in 10 mM Hepes buffer (pH 7.4) with 150 mM NaCl were injected via the tail vein either 3 times (Figure 2a) or 5 times (Figure 2b) at 4-day intervals. Gemcitabine and Avastin doses and injection regimens were according to the previous reports published elsewhere.[15,16] A polyplex micelle containing Luc pDNA was used as a control formulation containing the nontherapeutic gene. Tumor size was measured every second day by a digital vernier caliper across its longest (*a*) and shortest diameters (*b*), and its volume (*V*) was calculated according to the formula $V = 0.5ab^2$.

***In Vivo* sFlt-1 Gene Expression.** Polyplex micelles loading either sFlt-1 or Luc pDNA (20 μg pDNA) were injected into the BxPC3-inoculated mice via the tail vein on days 0 and 4. Mice were sacrificed on day 6 after collecting blood, and the lungs, livers, spleens, kidneys, and tumors were excised. The excised organs were treated in 500 μL of cell culture lysis buffer (Promega, Madison, WI), homogenized, and centrifuged. The sFlt-1 concentration of supernatants was evaluated using the immunoassay kit according to the manufacturer's protocol. Note that block copolymers and polyplex micelles did not interfere with ELISA (Figure 2 in the Supporting Information).

**Vascular Density in the Tumors.** Polyplex micelles loading either sFlt-1 or Luc pDNA (20 μg of pDNA) and Avastin (50 mg/kg) were injected into the BxPC3-inoculated

(14) Kim, W. J.; Yockman, J. W.; Lee, M.; Jeong, J. H.; Kim, Y. H.; Kim, S. W. Soluble Flt-1 Gene Delivery Using PEI-g-PEG-RGD Conjugate for Anti-angiogenesis. *J. Controlled Release* **2005**, *106*, 224–234.

(15) Braakhuis, B. J. M.; van Dongen, G. A. M. S.; Vermorken, J. B.; Snow, G. B. Preclinical In Vivo Activity 2′,2′-Difluorodeoxycytidine (Gemcitabine) against Human Head and Neck Cancer. *Cancer Res.* **1991**, *51*, 211–214.

(16) Gerber, H. P.; Ferrara, N. Pharmacology and Pharmacodynamics of Bevacizumab as Monotherapy or in Combination with Cytotoxic Therapy in Preclinical Studies. *Cancer Res.* **2005**, *65*, 671–680.

mice via the tail vein on days 0 and 4. Mice were sacrificed on day 6, and the tumors were excised, frozen in dry-iced acetone, and sectioned at 10 $\mu$m thickness in a cryostat. Vascular endothelial cells (VECs) were immunostained by rat monoclonal antibody antiplatelet endothelial cell adhesion molecule-1 (PECAM-1) (BD Pharmingen, Franklin Lakes, NJ) and Alexa488-conjugated secondary antibody. The samples were observed with a confocal laser scanning microscope (CLSM). The CLSM observation was performed using an LSM 510 (Carl Zeiss, Oberlochen, Germany) with an EC Plan-Neoflur 20× objective (Carl Zeiss) at the excitation wavelength of 488 nm (Ar laser). The PECAM-1-positive area (%) was calculated from Alexa488-positive pixels.

***In Vivo* EGFP Gene Expression in the Tumors.** Polyplex micelles loading EGFP pDNA (20 $\mu$g of pDNA) were injected into the BxPC3-inoculated mice via the tail vein. Mice were sacrificed on either day 3 or day 7. Tumors were excised, fixed with 10% formalin, frozen, and sectioned. VECs were immunostained by anti-PECAM-1 antibody and Alexa647-conjugated secondary antibody. After nuclear staining with Hoechst 33342, CLSM observation was carried out using the LSM 510 with the EC Plan-Neoflur 20× objective at the excitation wavelength of 488 nm for EGFP expression, 633 nm (He−Ne laser) for Alexa647, and 710 nm (MaiTai laser, two photon excitation; Spectra-Physics, Mountain View, CA) for Hoechst 33342, respectively. The representative images of tumors excised on day 3 are shown in Figure 5. Note that images of tumors excised on day 7 showed similar patterns to those on day 3, however with lower intensity of EGFP expression.

## Results

**Formation of Polyplex Micelles.** No free pDNA was detected by agarose gel electrophoresis, confirming that all pDNA was entrapped in disulfide cross-linked polyplex micelles, which were prepared as previously reported through ion complexation of block copolymers with pDNA at the N/P ratio = 2. Free thiol groups in polyplex micelles were estimated to be less than 2% by Ellman's test (data not shown), which is consistent with our previous report.[10] Weight−weight % ratios of pDNA/micelle in each formulation were as follows: 32.8% in B-SH0% formulation; 31.0% in B-SH5%; 29.2% in B-SH11%; 26.4% in B-SH20%; and 21.0% in B-SH36%. The mean size of the micelles was between 100 and 150 nm, with a moderate polydispersity index between 0.17 and 0.2 (Figure 3 in the Supporting Information), while zeta-potential revealed approximately neutral values, confirming the formation of PEG palisade surrounding the polyplex core (Table 1).

**Real-Time Gene Expression.** *In vitro* real-time Luc gene expression of polyplex micelles was evaluated using Kronos

***Table 1.*** Sizes and Zeta-Potentials of Polyplex Micelles with Various Cross-Linking Rates at N/P = 2[a]

| thiolation degree (%) | cumulant diameter (nm) | polydispersity index ($\mu/\Gamma^2$) | zeta-potential (mV) |
|---|---|---|---|
| 0 | 107 ± 2 | 0.195 ± 0.021 | 1.66 ± 0.28 |
| 5 | 117 ± 2 | 0.184 ± 0.011 | 1.25 ± 0.40 |
| 11 | 116 ± 2 | 0.171 ± 0.013 | 1.02 ± 0.30 |
| 20 | 139 ± 6 | 0.182 ± 0.050 | 0.40 ± 0.07 |
| 36 | 147 ± 2 | 0.192 ± 0.061 | −0.96 ± 0.02 |

[a] The results reported were expressed as mean ± SEM ($n$ = 3).

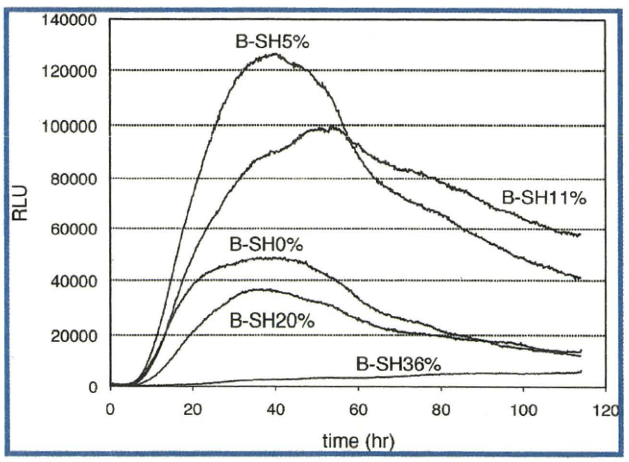


***Figure 1.*** Real-time luciferase gene expression of the polyplex micelles with varying thiolation degrees at N/P = 2 against 293T cells.

Dio for a prolonged period (Figure 1).[17,18] The B-SH5% cross-linked polyplex micelle showed the highest gene expression among all micelles until 60 h. Worth mentioning is that the transfection efficiency of the B-SH11% micelle continued to exceed that of the B-SH5% micelle after 60 h. Disulfide cross-links in the polyplex core are believed to contribute not only to enhanced stability of the micelles in the medium but also to sustained release of complexed pDNA inside the cells with a reductive environment, resulting in polyplex micelles with higher cross-linking rates that can maintain an appreciable transfection efficiency over a longer time scale. Note that the B-SH36% micelle showed an increasing trend in gene expression with time.

**Antitumor Activity.** Polyplex micelles containing sFlt-1 pDNA were injected iv into mice bearing pancreatic adenocarcinoma BxPC3, followed by evaluation of tumor volume (Figure 2). All the micelles were injected three times on days

(17) Takae, S.; Miyata, K.; Oba, M.; Ishii, T.; Nishiyama, N.; Itaka, K.; Yamasaki, Y.; Koyama, H.; Kataoka, K. PEG-detachable Polyplex Micelles Based on Disulfide-crosslinked Block Cationers as Bioresponsive Nonviral Gene Vectors. *J. Am. Chem. Soc.* **2008**, *130*, 6001–6009.

(18) Oba, M.; Aoyagi, K.; Miyata, K.; Matsumoto, Y.; Itaka, K.; Nishiyama, N.; Yamasaki, Y.; Koyama, H.; Kataoka, K. Polyplex Micelles with Cyclic RGD Peptide Ligands and Disulfide Cross-links Directing to the Enhanced Transfection via Controlled Intracellular Trafficking. *Mol. Pharmaceutics* **2008**, *5*, 1080–1092.

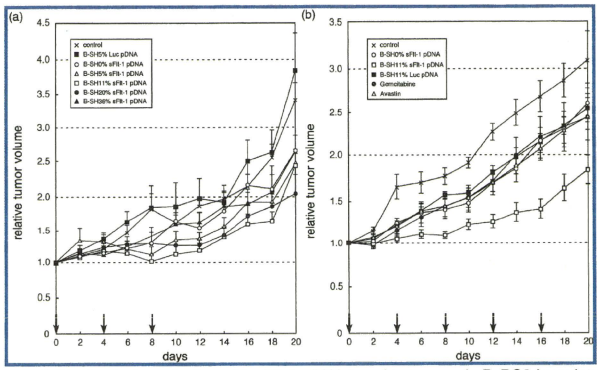


***Figure 2.*** Antitumor activity of polyplex micelles with sFlt-1 pDNA in subcutaneously BxPC3-inoculated mice. (a) Effect of thiolation degree. Hepes buffer (control) was used as a negative control. Polyplex micelles were injected iv on days 0, 4, and 8 at 20 $\mu$g pDNA/mouse, and mice were monitored for the relative tumor volume every second day. Error bars represent the SEM ($n = 6$). Only the B-SH11% polyplex micelles exhibited significant retardation of tumor growth compared to the control ($P < 0.01$). (b) Growth curve study with an increased dose of the B-SH11% polyplex micelles compared to commercially available drugs. Polyplex micelles (20 $\mu$g pDNA/mouse), gemcitabine (100 mg/kg), and Avastin (50 mg/kg) were injected iv on days 0, 4, 8, 12, and 16. Relative tumor size was measured every second day. Hepes buffer (control) was used as a negative control. Error bars represent the SEM ($n = 5$). Only the B-SH11% polyplex micelles exhibited significant retardation of tumor growth compared to the control ($P < 0.001$). $P$ values were calculated by multivariate ANOVA study.

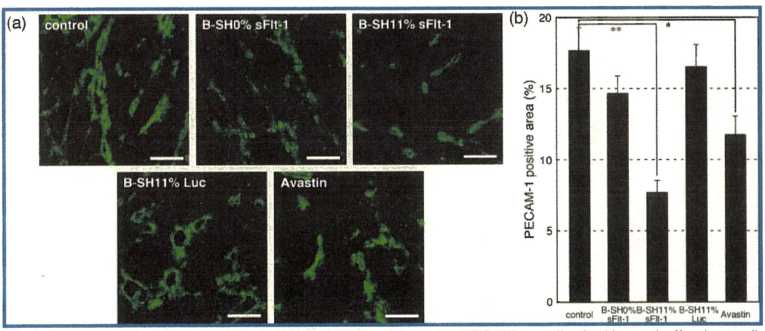


***Figure 3.*** Immunostaining of the VECs in the BxPC3 tumor tissue by PECAM-1 antibody. Hepes buffer (control), three types of polyplex micelles (20 $\mu$g of pDNA/mouse), and Avastin (50 mg/kg) were injected into the BxPC3-inoculated mice via the tail vein on days 0 and 4. Mice were sacrificed on day 6, and tumors were excised and immunostained. (a) CLSM images of immunostained tumors. PECAM-1-positive regions are green. Bars represent 100 $\mu$m. (b) Areas of PECM-1-positive endothelium were quantified. Error bars represent the SEM ($n = 15$). $P$ values were calculated by Student's $t$ test. $^*P < 0.01$ and $^{**}P < 0.001$.

0, 4, and 8 (Figure 2a). The B-SH11% micelle significantly suppressed tumor growth compared to control mice treated with Hepes buffer ($P < 0.01$). There was no significant change in tumor growth after injection of other polyplex micelles, implying that an optimal cross-linking rate is required to achieve an effective expression of the gene. Encouraged by these results, the tumor growth suppression activity of B-SH11% micelle was further evaluated, implying a regimen with enhanced number of injections. The effect of the micelles was compared to commercially available drugs, gemcitabine, a standard chemotherapeutic agent for pancreatic tumor, and bevacizumab (Avastin), a monoclonal antibody against VEGF (Figure 2b). The doses of gemcitabine and Avastin implied in our study were based on

previous reports published elsewhere.[15,16] The administration of B-SH11%/sFlt-1 micelle resulted in significant suppression of tumor growth ($P < 0.001$), while gemcitabine and Avastin, under the reported experimental regimen, showed no remarkable therapeutic effect. Note that the difference observed in tumor volumes between the B-SH11%/Luc micelle-treated group and the control group was not significant.

**Tumor Vascular Density.** The antiangiogenic effect of expressed sFlt-1 was confirmed by immunostaining of VECs using PECAM-1 (Figure 3). Vascular density of tumors treated with either B-SH11%/sFlt-1 micelle or Avastin was significantly lower than that of the other groups. The most pronounced and significant effect on neo-vasculature suppression was achieved by B-SH11%/sFlt-1 micelle (7% PECAM-1 positive area) over Avastin (12% PECAM-1 positive area) ($P < 0.05$). These results suggest that the expressed sFlt-1 may entrap VEGF secreted in the tumor tissue, thereby suppressing the growth of VECs.

***In Vivo* sFlt-1 Gene Expression.** Expression levels of sFlt-1 in the body were then evaluated by measuring the amount of sFlt-1 in lung, liver, spleen, kidney, tumor, and blood plasma using enzyme-linked immunosorbent assay (ELISA) (Figure 4). Injection of B-SH11%/sFlt-1 micelle resulted in significantly higher expression of sFlt-1 selectively in tumor tissue compared to the control. On the other hand, injection of B-SH0%/sFlt-1 micelle or B-SH11%/Luc micelle did not result in any difference in sFlt-1 expression compared to the control. These results strongly support that tumor-specific elevation in sFlt-1 expression led to the significant growth suppression of VECs in the tumor tissue and, eventually, the suppression of tumor growth.

***In Vivo* Enhanced Green Fluorescence Protein (EGFP) Gene Expression in Tumors.** The location of gene expression in BxPC3 tumors after administration of the micelles was analyzed histologically using pDNA encoding EGFP (Figure 5). As previously reported,[13,19,20] thick fibrotic tissue was formed around blood vessels (red) inside the stroma of BxPC3 tumors, and nests of tumor cells (region T) were scattered in the stroma (Figure 5a). The expression of EGFP (Figures 5b and 5c) was observed mainly in the VECs and cells in stromal regions adjacent to some vasculature, indicating that VECs and fibroblasts near some vasculature in the stroma, but not the tumor cells, were transfected. As seen in Figure 5a, there were thick fibrotic tissues around blood vessels in the BxPC3 xenograft,

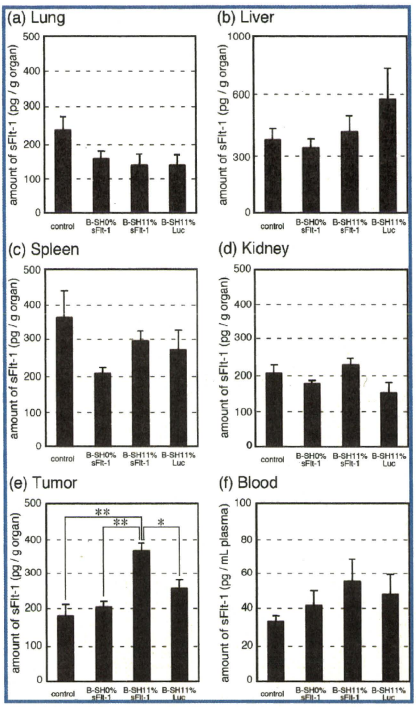


***Figure 4.*** Evaluation of sFlt-1 gene expression in organs by ELISA. Hepes buffer (control) and three types of polyplex micelles (20 $\mu$g pDNA/mouse) were injected into the BxPC3-inoculated mice via the tail vein on days 0 and 4. Mice were sacrificed on day 6 after collecting blood (f), and the lungs (a), livers (b), spleens (c), kidneys (d), and tumors (e) were excised, followed by evaluation of sFlt-1 concentration by ELISA according to the manufacturer's protocol. Error bars represent the SEM ($n = 6$). $P$ values were calculated by Student's $t$ test. $^*P < 0.01$ and $^{**}P < 0.001$.

indicating that the penetration of polyplex micelles deep into the stroma or into the tumor nest was interrupted and the gene expression was limited in the VECs and some of the fibroblasts in the stroma. Higher levels of EGFP expression were observed for B-SH11% micelle, confirming their enhanced ability to accumulate inside tumor tissue compared to B-SH0% micelle.

## Discussion

Since all solid tumors need angiogenesis for their growth, antiangiogenic therapy is a promising strategy for treating

(19) Miyata, K.; Oba, M.; Kano, M. R.; Fukushima, S.; Vachutinsky, Y.; Han, M.; Koyama, H.; Miyazono, K.; Nishiyama, N.; Kataoka, K. Polyplex Micelles from Triblock Copolymers Composed of Tandemly Aligned Segments with Biocompatible, Endosomal Escaping, and DNA-condensing Functions for Systemic Gene Delivery to Pancreatic Tumor Tissue. *Pharm. Res.* **2008**, *25*, 2924–2936.

(20) Kano, M. R.; Komuta, Y.; Iwata, K.; Oka, M.; Shirai, Y.; Morishita, Y.; Ouchi, Y.; Kataoka, K.; Miyazono, K. Comparison of the Effects of the Kinase Inhibitors Imatinib, Sorafenib, and Transforming Growth Factor-$\beta$ Receptor Inhibitor on Extravasation of Nanoparticles from Neovasculature. *Cancer Sci.* **2009**, *100*, 173–180.

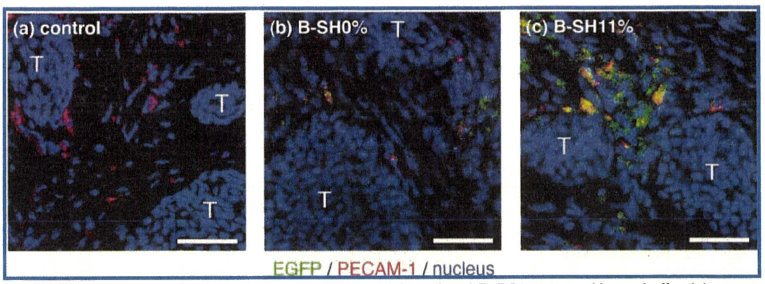


***Figure 5.*** EGFP gene expression by polyplex micelles in the inoculated BxPC3 tumors. Hepes buffer (a) was used as a negative control. B-SH0% (b) and B-SH11% (c) polyplex micelles containing EGFP pDNA (20 $\mu$g pDNA/mouse) were injected into the BxPC3-inoculated mice via the tail vein. Mice were sacrificed on day 3, and tumors were excised and immunostained. "T" indicates nests of tumor cells in tumor tissues. Bars represent 50 $\mu$m.

tumor patients. In fact, Avastin, the recombinant humanized monoclonal antibody against VEGF, has been widely used as an antiangiogenic drug, and its application range is spreading to the various types of solid tumors.[16] Other antiangiogenic proteins,[21,22] e.g., angiostatin, endostatin, and soluble forms of VEGF receptor, have also received great attention. Meanwhile, antiangiogenic gene therapy represents an attractive alternative to antiangiogenic proteins for reasons such as low dose, continuous expression of the therapeutic protein, and low cost. Therefore, development of an effective and safe gene vector is a key to successful antiangiogenic gene therapy.

In this study, thiolated PEG-PLys block copolymers were applied in the formation of disulfide cross-linked polyplex micelles for delivery of pDNA encoding sFlt-1, and tested for their antiangiogenic effect on mice bearing xenografted BxPC3 cell line, derived from human pancreatic adenocarcinoma. Disulfide cross-links in the polyplex core were designed to increase blood stability of the polyplex micelles and effectively release pDNA in the intracellular milieu.[10,11,18] PEG palisade of the polyplex micelle is expected to cover the polyplex core to shield the positive charge as well as to decrease interfacial free energy.[12,23] The formation of the PEG palisade surrounding the polyplex core was confirmed by the neutral zeta-potential of the polyplex micelles (Table 1). B-SH36% micelle showed an approximately 10 times higher concentration of pDNA in the blood at 60 min after iv injection than that of the micelle without core cross-linking (B-SH0%) (Figure 4 in the Supporting Information). The disulfide cross-links in the polyplex core apparently contribute to the enhanced stability of the micelles in the bloodstream. Note that the size of polyplex micelles is between 100 and 150 nm (Table 1), which may be in a suitable range for accumulation in solid tumors due to the enhanced permeability and retention (EPR) effect,[24] although the size may be too large to allow the micelles to penetrate into the stroma in pancreatic tumors.[13] Nevertheless, there is a concern that excessive disulfide cross-links interfere with the smooth release of entrapped pDNA in the core, resulting in decreased transfection efficiency.[10] Accordingly, optimal cross-linking density should be determined to balance the stability and maintain high transfection efficiency. The results of *in vitro* real-time gene expression showed that B-SH5% micelle possessed the highest efficiency among the evaluated samples up to 60 h after transfection. It is noteworthy that B-SH11% micelle exerted sustained Luc expression and kept an appreciably high efficiency beyond 60 h (Figure 1). Apparently, gene expression is prolonged with an increase in cross-linking rates, although excess cross-links induced overstabilization of polyplex micelles, resulting in decreased transfection efficiency in the case of the B-SH20% and B-SH36% micelles. Eventually, the B-SH36%/sFlt-1 micelle had no *in vivo* efficiency, even though they showed the highest stability in the bloodstream among the evaluated samples (Figure 4 in the Supporting Information). It is also noteworthy that the B-SH11%/sFlt-1 micelle achieved an appreciably high therapeutic efficiency, even though it showed only limited improvement in blood circulation time compared to the B-SH0% and B-SH5% systems. Presumably, a sustained

(21) Sim, B. K. L.; MacDonald, N. J.; Gubish, E. R. Angiostatin and Endostatin: Endogenous Inhibitors of Tumor Growth. *Cancer Metastasis Rev.* **2000**, *19*, 181–190.

(22) Fischer, C.; Mazzone, M.; Jonckx, B.; Carmeliet, P. FLT1 and Its Ligands VEGFB and PIGF: Drug Targets for Anti-angiogenic Therapy. *Nat. Rev. Cancer* **2008**, *8*, 942–956.

(23) Kakizawa, Y.; Kataoka, K. Block Copolymer Micelles for Delivery of Gene and Related Compounds. *Adv. Drug Delivery Rev.* **2002**, *54*, 203–222.

(24) Matsumura, Y.; Maeda, H. A New Concept for Macromolecular Therapeutics in Cancer Chemotherapy: Mechanism of Tumoritropic Accumulation of Proteins and the Antitumor Agent Smancs. *Cancer Res.* **1986**, *46*, 6387–6392.

profile in gene expression may have been the key to this achievement. Note that no change in body weight of the mice was observed during the experiment (data not shown), indicating few serious side effects of polyplex micelles.

Comparison with the commercially available agents, gemcitabine and Avastin, confirmed the encouraging tumor growth suppression effect of the B-SH11% polyplex micelle (Figure 2b). Gemcitabine continues to be the standard therapy in the treatment of pancreatic tumors; however, its objective response rate is limited in patients with advanced disease.[25] Avastin is a recombinant humanized monoclonal antibody against human VEGF, which may neutralize tumor-cell-derived VEGF in the model used here. In humans, Avastin is the first clinically available antiangiogenic drug, and it has been efficient when used in combined chemotherapy for metastatic colorectal cancer[26] and non-small-cell lung cancer.[27] However, it showed no benefit in patients with pancreatic tumors.[25] The B-SH11%/sFlt-1 micelle significantly suppressed tumor growth compared not only to the control ($P < 0.001$) but also to the B-SH11%/Luc micelle, gemcitabine, and Avastin ($P < 0.01$) (Figure 2b). Xenografted BxPC3 was reported not to respond to gemcitabine,[28] probably due to its inability to penetrate through the tumor thick fibrotic tissue and target tumor cells, which is consistent with our results. Evaluation of vascular density in BxPC3 tumor (Figure 3) clearly showed that the B-SH11%/sFlt-1 micelle decreased vascular density compared to the control ($P < 0.001$), the B-SH11%/Luc micelle ($P < 0.001$), and Avastin ($P < 0.05$) treated tumors.

Inhibitory effect on tumor growth (Figure 2) is consistent with the result of decreased vascular density. There are several studies on antiangiogenic gene therapy for subcutaneously inoculated tumors in mice by systemic expression of sFlt-1 using viral vectors, including im injection of adeno-associated viral vectors[29] and iv injection of adenoviral vectors to target livers.[30] In these studies, however, sFlt-1 was expressed mainly in organs rather than tumor tissue. What was worse, the excess expression of sFlt-1 in the liver led to unacceptable hepatotoxicity.[31] Thus, tumor-specific expression of sFlt-1 is essential for a safe and efficient antiangiogenic gene therapy. However, any nonviral gene vectors loading sFlt-1 gene have failed to exhibit selective gene expression in the tumor tissue, although they achieved certain inhibition of tumor growth.[8,9] In this regard, the B-SH11%/sFlt-1 micelle system might be promising, since sFlt-1 expression was significantly increased selectively in the tumor tissue compared not only to the control ($P < 0.001$) but also to the B-SH11%/Luc micelle ($P < 0.01$), as shown in Figure 4, without any significantly enhanced expression in other normal tissues. Note that no significant increase of sFlt-1 expression was observed in any normal organs treated with B-SH0%/sFlt-1 micelle or B-SH11%/Luc micelle. Histological analyses revealed that EGFP expression of the B-SH11%/EGFP micelle was located mainly around VECs but not in the tumor cells (Figure 5), probably due to restricted permeation of micelles by thick fibrotic tissues and pericyte-covered vasculature of the BxPC3 tumors. These results suggested the ability of expressed sFlt-1 molecule to entrap excess VEGF in the tumor tissue and to inhibit tumor growth by an antiangiogenic effect. Xenografted BxPC3 tumors in mice are characterized by stroma-rich histology,[20] which might explain the only slight inhibitory effects on BxPC3 growth achieved by gemecitabine[28] targeting tumor cells.

## Conclusions

In conclusion, antiangiogenic gene therapeutic study was carried out by iv administration of polyplex micelles with sFlt-1 pDNA to mice bearing pancreatic adenocarcinoma BxPC3 xenografts, and the results demonstrated the ability of B-SH11% sFlt-1 micelle as a safe and effective gene delivery system. The optimal disulfide cross-linking rate of polyplex micelles was found to show significant suppression of tumor growth. Gene expression of sFlt-1 by iv injection of polyplex micelles was observed in tumor tissue only, followed by decreased vascular density and significant suppression of tumor growth. Based on these results, the B-SH11% disulfide cross-linked polyplex

(25) Rocha-Lima, C. M. New Directions in the Management of Advanced Pancreatic Cancer: a Review. *Anti-Cancer Drugs* **2008**, *19*, 435–446.

(26) Hurwitz, H.; Fehrenbacher, L.; Novotny, W.; Cartwright, T.; Hainsworth, J.; Heim, W.; Berlin, J.; Baron, A.; Griffing, S.; Holmgren, E.; Ferrara, N.; Fyfe, G.; Rogers, B.; Ross, R.; Kabbinavar, F. Bevacizumab Plus Irinotecan, Fluorouracil, and Leucovorin for Metastatic Colorectal Cancer. *N. Engl. J. Med.* **2004**, *350*, 2335–2342.

(27) Sandler, A.; Gray, R.; Perry, M. C.; Brahmer, J.; Schiller, J. H.; Dowlati, A.; Lilenbaum, R.; Johnson, D. H. Paclitaxel-carboplatin Alone or with Bevacizumab for Non-small-cell Lung Cancer. *N. Engl. J. Med.* **2006**, *355*, 2542–2550.

(28) Merriman, R. L.; Hertel, L. W.; Schultz, R. M.; Houghton, P. J.; Houghton, J. A.; Rutherford, P. G.; Tanzer, L. R.; Boder, G. B.; Grindey, G. B. Comparison of the Antitumor Activity of Gemcitabine and Ara-C in a Panel of Human Breast, Colon, Lung and Pancreatic Xenograft Models. *Invest. New Drugs* **1996**, *14*, 243–247.

(29) Takei, Y.; Mizukami, H.; Saga, Y.; Yoshimura, I.; Hasumi, Y.; Takayama, T.; Kohno, T.; Matsushita, T.; Okada, T.; Kume, A.; Suzuki, M.; Ozawa, K. Suppression of Ovarian Cancer by Muscle-Mediated Expression of Soluble VEGFR-1/Flt-1 Using Adeno-associated Virus Serotype 1-derived Vector. *Int. J. Cancer* **2006**, *120*, 278–284.

(30) Liu, J.; Li, J.; Su, C.; Huang, B.; Luo, S. Soluble Fms-like Tyrosine Kinase-1 Expression Inhibits the Growth of Multiple Myeloma in Nude Mice. *Acta Biochim. Biophys. Sin.* **2007**, *39*, 499–506.

(31) Mahasreshti, P. J.; Kataram, M.; Wang, M. H.; Stockard, C. R.; Grizzle, W. E.; Carey, D.; Siegal, G. P.; Haisma, H. J.; Alvarez, R. D.; Curiel, D. T. Intravenous Delivery of Adenovirus-mediated Soluble FLT-1 Results in Liver Toxicity. *Clin. Cancer Res.* **2003**, *9*, 2701–2710.

micelle with sFlt-1 pDNA is interesting and worthy to develop further for antiangiogenic gene therapy of solid tumors.

**Acknowledgment.** This work was financially supported in part by the Core Research Program for Evolutional Science and Technology (CREST) from Japan Science and Technology Agency (JST) as well as by Grants-in-Aid for Young Scientists (A) and Exploratory Research. We express our appreciation to Masabumi Shibuya (Tokyo Medical and Dental University) for providing pVL 1393 baculovirus vector pDNA encoding human sFlt-1. We thank Kazuhiro Aoyagi, Yoko Hasegawa, Kotoe Date, and Satomi Ogura (The University of Tokyo) for technical assistance.

**Supporting Information Available:** Synthesis of thiolated block copolymer and Supporting Figures 1, 2, 3, and 4. This material is available free of charge via the Internet at http://pubs.acs.org.

MP9002317

Antibody Delivery

DOI: 10.1002/anie.200905264

# Efficient Delivery of Bioactive Antibodies into the Cytoplasm of Living Cells by Charge-Conversional Polyion Complex Micelles**

*Yan Lee, Takehiko Ishii, Hyun Jin Kim, Nobuhiro Nishiyama, Yoshiyuki Hayakawa, Keiji Itaka, and Kazunori Kataoka**

Antibodies are the most important component of humoral immunity, and can recognize and deactivate their corresponding extracellular antigens with outstanding selectivity. Moreover, the development of monoclonal and humanized antibodies has contributed greatly to the recent success of antibodies as biopharmaceuticals.[1] However, the target of such antibodies is limited to the cell exterior because of the lack of a delivery system of antibodies into the interior of the cell. Although the detection or inactivation of an intracellular protein was partially accomplished by the intracellular expression of antibodies,[2] the development of an efficient and safe delivery method of an antibody into living cells is required for further advances in therapeutics and bioanalysis. Various methods, such as microinjection, liposomes, cell-penetrating peptides, and even recombinant viruses, have been introduced;[3] however, their general use is often limited because of the need for highly specialized devices, as well as the complexity and inefficiency of these methods.

We recently developed a novel protein-delivery system into cytoplasm based on charge-conversional polyion complex (PIC) micelles.[4] The charge density of a model protein, cytochrome *c*, can be temporarily increased by the modification of the ε-amines of lysine residues into charge-conversional moieties, citraconic acid amide (Cit) or *cis*-aconitic acid amide (Aco) (Figure 1). As the positively charged lysines convert to the negatively charged carboxylic groups by this modification, the modified proteins become strongly anionic and the resulting charge density can be increased significantly to form stable PIC micelles with cationic block copolymers even at physiological salt concentrations. The charge-converted proteins and the cationic block in the copolymer form the core of the PIC micelle, and the polyethylene glycol (PEG) block forms the surface shell. After the PIC micelles were internalized to cells, the Cit and Aco rapidly degraded to reproduce the original lysines at the endosomal pH of 5.5.[5] The dissociation of the PIC micelles follows the regeneration of the original protein to release the free cationic block copolymer, which induces the pH-dependent destabilization

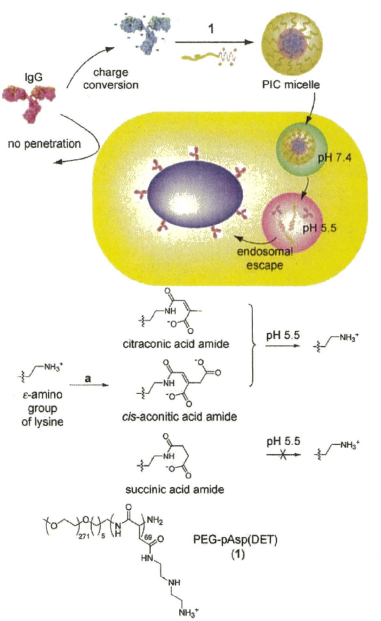


***Figure 1.*** Preparation of the charge-conversional PIC micelles between IgG derivatives and PEG-pAsp(DET). a) Citraconic anhydride, *cis*-aconitic anhydride, or succinic anhydride. IgG = immunoglobulin G, PEG-pAsp(DET) = PEG-poly{*N*-[*N*'-(2-aminoethyl)-2-aminoethyl]aspartamide}.

[*] Dr. T. Ishii, Prof. Dr. K. Kataoka
Department of Bioengineering, The University of Tokyo
7-3-1 Hongo, Bunkyo-ku, Tokyo 113-8656 (Japan)
Fax: (+81) 3-5841-7139
E-mail: kataoka@bmw.t.u-tokyo.ac.jp
Dr. Y. Lee
Department of Chemistry, Seoul National University
Sillim-dong, Gwanak-gu, Seoul 151-742 (Korea)
H. J. Kim, Y. Hayakawa, Prof. Dr. K. Kataoka
Department of Materials Engineering
The University of Tokyo (Japan)
Dr. N. Nishiyama, Dr. K. Itaka, Prof. Dr. K. Kataoka
Center for Disease Biology and Integrative Medicine
Graduate School of Medicine, The University of Tokyo (Japan)
Dr. N. Nishiyama, Dr. K. Itaka, Prof. Dr. K. Kataoka
Center for Nanobio Integration, The University of Tokyo (Japan)

[**] This work was supported by a Core Research for Evolutional Science and Technology (CREST) grant from the Japan Science and Technology Agency (JST).

Supporting information for this article is available on the WWW under http://dx.doi.org/10.1002/anie.200905264.

of the endosomal membrane to aid the endosomal escape of the protein into cytoplasm.[6]

In the present study, we applied the same concept to intracellular antibody delivery for the purpose of controlling a cell pathway. As the molecular weight of the PIC micelle is well over several megadaltons,[7] we expected that the charge-conversional PIC micelle could easily deliver full immunoglobulin G (IgG) molecules with a molecular weight of 150 kD, which are difficult to deliver into the cytoplasm of living cells.

First, we examined the change in bioselectivity after the charge-conversional modification of IgG by using fixed and permeated cells in which the plasma membrane is no longer a penetration barrier of antibodies. All experimental procedures are described in detail in the Supporting Information. The nuclear pore complex (NPC), which is a protein complex that controls the transport of biomolecules across the nuclear envelope, was selected as a target for the antibodies.[8] Although anti-NPC mouse IgG can recognize the NPC of fixed cells selectively (Supporting Information, Figure S1a), anti-NPC IgG modified with Cit (anti-NPC IgG-Cit) loses this selectivity (Supporting Information, Figure S1b). However, the selectivity of anti-NPC IgG-Cit is mostly recovered after incubation at pH 5.5 (Figure 2b), contrary to the result after

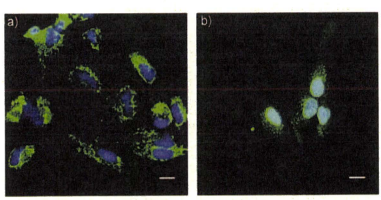


***Figure 2.*** Recognition of NPC in fixed human hepatoma (HuH-7) cells by anti-NPC IgG-Cit after 4 h of incubation at a) pH 7.4 and b) pH 5.5. Anti-NPC IgG-Cit was applied to the cells after fixation. The cell nuclei were stained by Hoechst 33258 (blue), and the anti-NPC IgG-Cit was detected by a secondary antibody, the Alexa Fluor 488-labeled $(Fab')_2$ fragment from goat anti-mouse IgG (green). Scale bars: 20 μm. Fab = fragment, antigen-binding.

incubation at pH 7.4 (Figure 2a). The rapid degradation of Cit at pH 5.5 allowed regeneration of the selectivity of anti-NPC IgG. The selectivity change of the other derivatives, anti-NPC IgG modified with Aco (anti-NPC IgG-Aco) and anti-NPC IgG modified with a nondegradable succinic acid amide (anti-NPC IgG-Suc), is shown in Figure S1 in the Supporting Information. As expected, nondegradable anti-NPC IgG-Suc showed no selectivity after incubation at either pH 7.4 or pH 5.5.

For the formation of PIC micelles, we selected PEG-poly{*N*-[*N'*-(2-aminoethyl)-2-aminoethyl]aspartamide} (PEG-pAsp(DET); **1**) as a cationic block copolymer. Compound **1** shows efficient cytoplasmic delivery of DNA and proteins with minimal cytotoxicity,[9] and thus we expected that the PIC micelles based on **1** would also be able to deliver IgG into cytoplasm efficiently. The formation of PIC micelles between the modified anti-NPC IgG derivatives and **1** was examined by dynamic light scattering (DLS; Table 1).

***Table 1:*** Formation of PIC micelles containing IgG derivatives.

| IgG derivative | Diameter [nm][a] | PDI[a,b] |
|---|---|---|
| anti-NPC IgG | N.D.[c] | N.D. |
| anti-NPC IgG-Cit | 98.3 | 0.096 |
| anti-NPC IgG-Aco | 107 | 0.016 |
| anti-NPC IgG-Suc | 111 | 0.121 |

[a] Determined by DLS. [b] Polydispersity index. [c] Not determined.

Although the native anti-NPC IgG could not form the PIC micelles with **1**, anti-NPC IgG derivatives with increased charge densities were able to form PIC micelles successfully, even at physiological salt concentrations (150 mM NaCl). All PIC micelles showed unimodal size distributions (Supporting Information, Figure S2) with hydrodynamic diameters of around 100 nm.

The pH-dependent dissociation of the charge-conversional PIC micelles containing the antibody derivatives was confirmed by the fluorescence quenching/dequenching method.[10] Herein, we used Alexa Fluor 488-labeled IgG $(Fab')_2$ fragments from goat anti-mouse IgG as a payload in the PIC micelles instead of whole IgG molecules to chase the green fluorescence. The fluorescence intensity of the IgG $(Fab')_2$ derivatives in the core of the PIC micelles was reduced significantly as a result of the probe–probe quenching effect (20–30%). The decreased fluorescence intensity could be recovered after the release of the IgG $(Fab')_2$ from the PIC micelles (Supporting Information, Figure S4). Although the PIC micelles containing IgG $(Fab')_2$-Cit or IgG $(Fab')_2$-Aco were stable at pH 7.4, they dissociated rapidly at pH 5.5. The decrease of the charge density in IgG $(Fab')_2$ derivatives resulting from the pH-sensitive degradation of Cit and Aco is likely to be the main reason for this destabilization.

Next, we examined the intracellular trafficking of the charge-conversional antibodies on the living cells without fixation or permeation. Because the encapsulated IgG $(Fab')_2$ derivatives were labeled with Alexa Fluor 488 (green) and the late endosomes and lysosomes were stained with Lysotracker Red (red), the IgG $(Fab')_2$ in the endosome showed yellow fluorescence as a result of the co-localization of green and red fluorescence. The IgG $(Fab')_2$ was detected as green only after endosomal escape. IgG $(Fab')_2$-Cit showed efficient endosomal escape (Figure 3a), whereas IgG $(Fab')_2$-Aco and IgG $(Fab')_2$-Suc showed limited endosomal escape (Figure 3b,c). The degrees of endosomal escape are summarized in Figure 3d as a co-localization ratio between the green and red fluorescence; the lower the co-localization ratio, the more efficient the endosomal escape. The most efficient endosomal escape of the Cit derivative corresponds to our previous result.[4b] Because pH-sensitive protonation and direct contact with the endosomal membrane of the pAsp(DET) block are essential for endosomal destabilization,[11] the lowest endosomal escape of the nondissociable IgG $(Fab')_2$-Suc PIC micelle is reasonable.

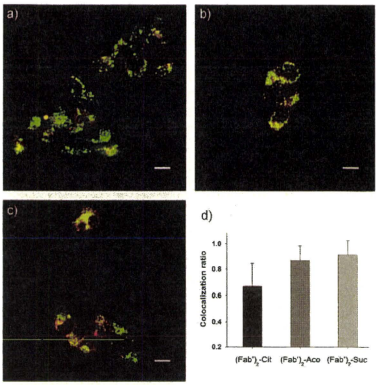


***Figure 3.*** Confocal laser scanning microscopy (CLSM) images of HuH-7 cells treated with PIC micelles containing Alexa Fluor 488-labeled IgG $(Fab')_2$ fragment derivatives (green). a) $(Fab')_2$-Cit, b) $(Fab')_2$-Aco, and c) $(Fab')_2$-Suc. The late endosomes and lysosomes were stained with LysoTracker Red. Scale bars: 20 μm. d) Colocalization of the green fluorescence of $(Fab')_2$ derivatives and the red fluorescence of LysoTracker Red. Error bars: standard deviation.

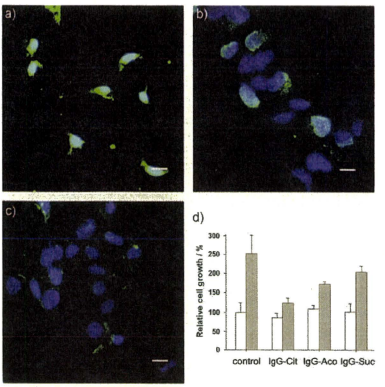


***Figure 4.*** CLSM images of HuH-7 cells treated with PIC micelles containing a) anti-NPC IgG-Cit, b) anti-NPC IgG-Aco, and c) anti-NPC IgG-Suc. The cell nuclei were stained by Hoechst 33258 (blue), and the IgG derivatives were detected by a secondary antibody, the Alexa Fluor 488-labeled $(Fab')_2$ fragment from goat anti-mouse IgG (green). Scale bars: 20 μm. d) Growth of HuH-7 cells treated by each type of PIC micelle. White and gray bars represent the relative cell growth after 24 and 48 h of incubation, respectively. Error bars: standard deviation.

Finally, we examined the recognition of the NPC by the intracellular delivery of anti-NPC IgG into living cells by PIC micelles. The intracellular distribution of anti-NPC IgG released from the micelles was visualized by treating the cells with a secondary antibody, the Alexa Fluor 488-labeled $(Fab')_2$ fragment from goat anti-mouse IgG (green), after fixation. Note that the IgG derivative segregated in the core of PIC micelles may not be detected by this procedure; however, the released IgG can be selectively visualized in the cell. Anti-NPC IgG-Cit showed excellent recognition activity of NPC compared to the other IgG derivatives. The strong aquamarine fluorescence from the co-localization of the anti-NPC IgG (green) and the nucleus (blue) clearly represents NPC recognition by the anti-NPC IgG released from the anti-NPC IgG-Cit PIC micelles (Figure 4a). Anti-NPC IgG-Aco also recognized the NPC, but the intensity of its green fluorescence was lower than that of anti-NPC IgG-Cit, probably because of its limited endosomal escape efficiency (Figure 4b). The non-charge-conversional control, anti-NPC IgG-Suc, showed no selectivity on the nuclear envelope (Figure 4c).

The control of cell growth by the delivery of charge-conversional intracellular antibodies was confirmed by counting cell numbers (Figure 4d). As NPC controls the transport of essential biomolecules between the nucleoplasm and cytoplasm, the recognition and deactivation of NPC by anti-NPC IgG are critical for cell growth. Cells that were treated with anti-NPC IgG-Suc PIC micelles showed almost no change in cell growth, whereas those treated with anti-NPC IgG-Cit micelles showed a significant reduction in cell growth ($P < 0.05$) after 48 h. The effect of the anti-NPC IgG-Aco PIC micelles was midway between those of anti-NPC IgG-Cit and anti-NPC IgG-Suc. A comparison with control data from a nonspecific IgG (IgG1 kappa) is shown in Figure S6 in the Supporting Information.

In summary, we have successfully delivered biologically active IgG into cytoplasm by the charge-conversional PIC micelle method for controlling cell growth. Considering that an antibody has outstanding selectivity on its corresponding antigen, the concept of charge-conversional intracellular antibody delivery reported here is expected to have high potential for the bioimaging of the intracellular structures and functions of living cells, as well as for biotherapeutics to target intracellular antigens. Moreover, charge-conversional PIC micelles could be used in intravenous protein delivery, based on the high biocompatibility and elongated circulation provided by the PEG shell of the PIC micelles. New therapeutic strategies with both specificity and efficiency may also be expected through the combination of an antibody-based ligand for the recognition of a specific extracellular antigen on the cell surface and the charge-conversional antibody for the deactivation of an intracellular antigen.

Received: September 21, 2009
Published online: March 5, 2010

**Keywords:** antibodies · biological activity · charge conversion · drug delivery · micelles

  

[1] a) G. Köhler, C. Milstein, *Nature* **1975**, *256*, 495–497; b) M. J. Glennie, J. G. J. van de Winckel, *Drug Discovery Today* **2003**, *8*, 503–510; c) R. A. Lerner, *Angew. Chem.* **2006**, *118*, 8284–8305; *Angew. Chem. Int. Ed.* **2006**, *45*, 8106–8125.

[2] M. Stocks, *Curr. Opin. Chem. Biol.* **2005**, *9*, 359–365.

[3] a) K. H. Antman, D. M. Livingston, *Cell* **1980**, *19*, 627–635; b) C. A. Lackey, O. W. Press, A. S. Hoffman, P. S. Stayton, *Bioconjugate Chem.* **2002**, *13*, 996–1001; c) M. C. Morris, J. Depollier, J. Mery, F. Heitz, G. Divita, *Nat. Biotechnol.* **2001**, *19*, 1173–1176; d) B. Cornelissen, M. Hu, K. McLarty, R. M. Reilly, *Nucl. Med. Biol.* **2007**, *34*, 37–46; e) Y. Kondo, K. Fushikida, T. Fujieda, K. Sakai, K. Miyata, F. Kato, M. Kato, *J. Immunol. Methods* **2008**, *332*, 10–17.

[4] a) Y. Lee, S. Fukushima, Y. Bae, S. Hiki, T. Ishii, K. Kataoka, *J. Am. Chem. Soc.* **2007**, *129*, 5362–5363; b) Y. Lee, T. Ishii, H. Cabral, H. J. Kim, J. H. Seo, N. Nishiyama, H. Oshima, K. Osada, K. Kataoka, *Angew. Chem.* **2009**, *121*, 5413–5416; *Angew. Chem. Int. Ed.* **2009**, *48*, 5309–5312.

[5] a) J. K. Shetty, J. E. Kinsella, *Biochem. J.* **1980**, *191*, 269–272; b) Y. Lee, K. Miyata, M. Oba, T. Ishii, S. Fukushima, M. Han, H. Koyama, N. Nishiyama, K. Kataoka, *Angew. Chem.* **2008**, *120*, 5241–5244; *Angew. Chem. Int. Ed.* **2008**, *47*, 5163–5166.

[6] K. Miyata, M. Oba, M. Nakanishi, S. Fukushima, Y. Yamasaki, H. Koyama, N. Nishiyama, K. Kataoka, *J. Am. Chem. Soc.* **2008**, *130*, 16287–16294.

[7] A. Harada, K. Kataoka, *Macromolecules* **1998**, *31*, 288–294.

[8] K. J. Ryan, S. R. Wente, *Curr. Opin. Cell Biol.* **2000**, *12*, 361–371.

[9] a) N. Kanayama, S. Fukushima, N. Nishiyama, K. Itaka, W.-D. Jang, K. Miyata, Y. Yamasaki, U.-I. Chung, K. Kataoka, *ChemMedChem* **2006**, *1*, 439–444; b) K. Masago, K. Itaka, N. Nishiyama, U. Chung, K. Kataoka, *Biomaterials* **2007**, *28*, 5169–5175.

[10] a) B. Z. Packard, A. Komoriya, D. D. Toptygin, L. Brand, *J. Phys. Chem. B* **1997**, *101*, 5070–5074; b) Y. Lee, H. Mo, H. Koo, J.-Y. Park, M. Y. Cho, G. Jin, J.-S. Park, *Bioconjugate Chem.* **2007**, *18*, 13–18.

[11] S. Takae, K. Miyata, M. Oba, T. Ishii, N. Nishiyama, K. Itaka, Y. Yamasaki, H. Koyama, K. Kataoka, *J. Am. Chem. Soc.* **2008**, *130*, 6001–6009.

  